

Increasing the Bioavailability of Ru^{III} Anticancer Complexes through Hydrophobic Albumin Interactions

Michael I. Webb,^[a] Boris Wu,^[a] Thalia Jang,^[a] Ryan A. Chard,^[a] Edwin W. Y. Wong,^[a] May Q. Wong,^[b] Donald T. T. Yapp,^[b] and Charles J. Walsby*^[a]

Abstract: A series of pyridine-based derivatives of the clinically successful Ru^{III}-based complexes indazolium [*trans*-RuCl₄(1*H*-indazole)₂] (KP1019) and sodium [*trans*-RuCl₄(1*H*-indazole)₂] (KP1339) have been synthesized to probe the effect of hydrophobic interactions with human serum albumin (hsA) on anticancer activity. The solution behavior and protein interactions of the new compounds were characterized by using electron paramagnetic resonance (EPR) and UV/Vis spectroscopy. These studies have revealed that incorporation of hydrophobic substituents at the 4'-position of the axial pyridine ligand stabilizes non-coordinate interactions with hsA. As a consequence, direct coordination to the pro-

tein is inhibited, which is expected to increase the bioavailability of the complexes, thus potentially leading to improved anticancer activity. By using this approach, the lifetimes of hydrophobic protein interactions were extended from 2 h for the unsubstituted pyridine complex, to more than 24 h for several derivatives. Free complexes were tested for their anticancer activity against the SW480 human colon carcinoma cell line, exhibiting low cytotoxicity. Pre-treatment with hsA improved the solubility of every compound and

led to some changes in activity. Particularly notable was the difference in activity between the methyl- and dibenzyl-functionalized complexes. The former shows reduced activity after incubation with hsA, indicating reduced bioavailability due to protein coordination. The latter exhibits little activity on its own but, following treatment with hsA, exhibited significant cytotoxicity, which is consistent with its ability to form non-coordinate interactions with the protein. Overall, our studies demonstrate that non-coordinate interactions with hsA are a viable target for enhancing the activity of Ru^{III}-based complexes in vivo.

Keywords: albumin • cytotoxicity • hydrophobic interactions • ligand design • ruthenium

Introduction

Ruthenium compounds are drawing increasing attention as the next generation of metal-based anticancer agents.^[1] Clinical studies of Ru chemotherapeutics have reported significant antineoplastic and antimetastatic activity, with very low levels of side effects.^[2] The on-going development of Ru-based anticancer complexes is promoted by their fundamental chemical properties, which include 1) variable ligand-exchange rates, which are typically favorable with respect to rates of cell division,^[3] 2) a range of oxidation states, which are accessible under physiological conditions (i.e., II–IV),^[4] and 3) properties which are tunable by ligand design.^[5]

Amongst the most promising ruthenium-based drug candidates are negatively charged octahedral Ru^{III} complexes with axial azole ligands, an equatorial plane of chloride ligands, and charge compensation provided either by the protonated forms of the azole ligands or sodium ions (Figure 1).^[6] These compounds were first described by Keppler and co-workers in the early 1990s,^[7] and continue to serve as the benchmark for activity in the development of new Ru-based anticancer agents. “Keppler-type” complexes typically exhibit conventional antineoplastic properties and have demonstrated significant activity in colorectal cancer cell lines.^[8] One such compound, indazolium [*trans*-RuCl₄(1*H*-indazole)₂] (KP1019) (Figure 1) has drawn particular attention after successfully completing phase I clinical trials.^[2a,8b] Although KP1019 ultimately failed in phase II trials, primarily due to its poor solubility,^[9] further clinical development of its more soluble sodium-compensated analogue, KP1339 (Figure 1), is continuing.^[8c,10]

Significant effort has been expended to uncover the biological targets and anticancer mechanisms of Keppler-type compounds by using an array of analytical methods.^[9,11] Although their specific mode of action remains unclear, it is widely accepted that these complexes are prodrugs, with aqueous ligand exchange playing a significant role in their physiological speciation.^[8b] Although their azole ligands are

[a] Dr. M. I. Webb, B. Wu, T. Jang, R. A. Chard, Dr. E. W. Y. Wong, Prof. C. J. Walsby
Department of Chemistry, Simon Fraser University
Burnaby, BC, V5A 1S6 (Canada)
Fax: (+1) 778-782-3765
E-mail: cwalsby@sfu.ca

[b] M. Q. Wong, Dr. D. T. T. Yapp
Department of Experimental Therapeutics
BC Cancer Agency
Vancouver, BC, V5Z 4E6 (Canada)

Supporting information for this article is available on the WWW under <http://dx.doi.org/10.1002/chem.201302671>.

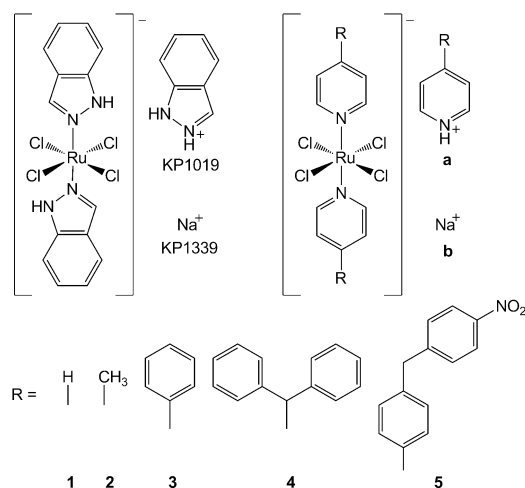


Figure 1. The Keppler-type Ru^{III}-based anticancer agents undergoing clinical evaluation, KP1019 and KP1339, and their pyridine-based analogues synthesized in this study.

generally kinetically inert,^[11g,12] the chloride ligands of these complexes readily exchange in aqueous solution, a process that has a direct impact on the activity of the complexes by generating aquated species.^[11b,e,13] In the case of KP1019, aqueous exchange is particularly significant because the mono-aqua derivative of the complex is insoluble and rapidly precipitates out of solution.^[14]

Under physiological conditions, Keppler-type complexes have been shown to bind readily to serum proteins,^[15] in particular to human serum albumin (hsA).^[11c,f,16] For KP1019 the presence of serum proteins inhibits its precipitation due to the formation of soluble protein-bound species.^[11b] In the case of hsA, the complexes can bind either through direct coordination to amino acid side chains,^[6,8b,14b,15,17] or in a non-coordinate fashion, likely within the hydrophobic binding domains of the protein^[18] as found in Sudlow's sites I and II.^[19]

We have previously used electron paramagnetic resonance (EPR) spectroscopy to characterize both coordinate and non-coordinate interactions of KP1019, and its cytotoxic imidazole analogue, imidazolium [*trans*-RuCl₄(1*H*-imidazole)₂] (KP418), with hsA.^[14b] These studies have shown that the axial heterocyclic ligands of these complexes play a central role in their protein binding behavior. KP1019 forms non-coordinate interactions with hsA very rapidly, with the resulting species converted readily to protein-coordinated complexes over time.^[14b] By contrast, KP418 slowly forms non-coordinate interactions with hsA following aqueous ligand exchange. These interactions are persistent and the formation of coordinated species does not occur even after prolonged incubation with the protein.^[14b,20] The ability of KP1019 to rapidly form non-coordinate interactions with hsA has been attributed to enhanced interactions of its indazole ligands with the hydrophobic domains of hsA,^[14b] as compared to the imidazole ligands of KP418.^[20] This has been implicated in the lower side effects of KP1019.^[5c,14b]

Overall, these observations have suggested that interactions with hsA can be tuned by the properties of the axial ligands.

Based on these observations, we have hypothesized that the bioavailability of Keppler-type complexes could be enhanced by promoting the hydrophobic interactions with hsA and consequently inhibiting the formation of coordinated species. To explore this concept we have synthesized a series of pyridine-based KP1019/1339 analogues. These compounds have a range of substituents at the 4'-position of the axial pyridine ligands, generating complexes with different tendencies to interact with the hydrophobic regions of hsA. The ligands chosen for these studies were: pyridine (Pyr, **1**), 4-methylpyridine (MePyr, **2**), 4-phenylpyridine (PhPyr, **3**), diphenyl-4-pyridyl-methane (DiPhenPyr, **4**), and 4-(4-nitrobenzyl)pyridine (NBenzPyr, **5**) (Figure 1). EPR and UV/Vis spectroscopy has been used to monitor how each of these ligands impacts on protein binding. We found that the different substituents have a marked effect on the stability of non-coordinate interactions, which correlates with their anticipated ability to interact with hydrophobic protein regions. Each complex was synthesized with both protonated pyridine ligands (series **a**) and sodium (series **b**) as compensating cations (Figure 1). The latter were required to make the compounds sufficiently soluble for testing of their anticancer activity.

To see how the improved stability of the hydrophobic interactions correlates with anticancer activity, we have tested the compounds against the SW480 human colon carcinoma cell line. In these experiments, we have screened the complexes both after preparation in buffered solution and following initial incubation with hsA. These studies indicate that the enhancement of non-coordinate interactions can improve the activity of the complexes both through inhibition of protein coordination and by increasing solubility.

Results and Discussion

Synthesis: Compounds **1a–5a** and **1b–5b** were synthesized by using procedures derived from the original syntheses of KP1019 and KP1339, respectively.^[7] An alternative synthesis and characterization of complex **1a** has been described elsewhere.^[21] However, this is the first report of the sodium analogue of this compound (i.e., compound **1b**) and all the other complexes, with either type of counterion. The identity and purity of the compounds was confirmed by elemental analysis, NMR, and EPR spectroscopy as well as X-ray crystallography analysis.

There have been a number of reports of derivatives of Ru^{III}-based Keppler-type complexes with different heterocyclic nitrogen ligands.^[22] However, to the best of our knowledge, this is the first study using systematic functionalization at a single position on the coordinated heterocyclic ligands to manipulate the properties of the complexes.

Crystal structures: The structures of compounds **1a**, **2a**, **3b**, **4a**, and **5a** were determined by X-ray crystallography and

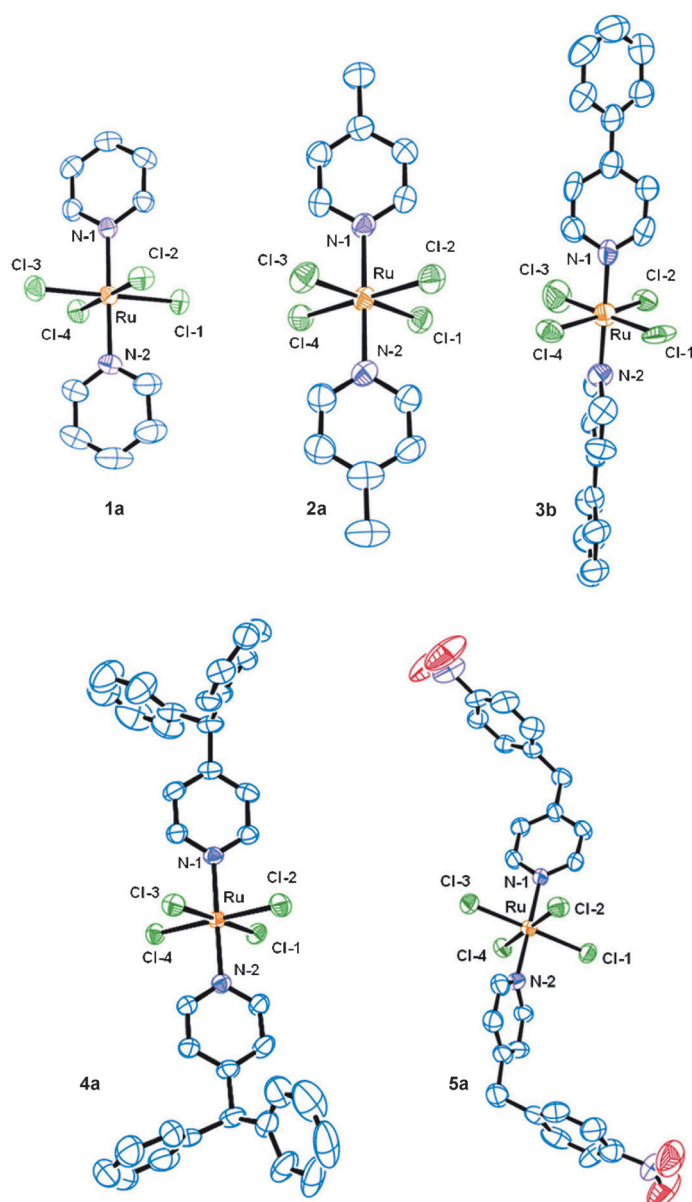


Figure 2. Crystal structures of the anions of complexes **1a**, **2a**, **3b**, **4a**, and **5a**. Structures are drawn at the 50% probability level. Counterions as well as coordinated solvent molecules are omitted for clarity.

are shown in Figure 2. For clarity, the counterions for each complex are omitted, along with any additional co-crystallizing solvent molecules. The diverse properties of the axial ligands required a variety of solvent conditions to produce suitably diffracting crystals. The structure of each anion type was determined, and other spectroscopic and analytical techniques were used to confirm the synthesis of the compounds with the alternate counterions. The crystal structure of complex **1a** has been described previously,^[21] but none of the other compounds have been reported or characterized crystallographically.

For all of the structures solved, a similar distorted octahedral geometry is observed. The bond lengths around the

ruthenium metal center for all of the complexes are listed in Table S4 in the Supporting Information. In all cases the two pyridine ligands are coordinated *trans* through the heterocyclic nitrogen atom with an average Ru–N bond length of 2.097 Å, which is slightly longer than the reported value for both KP418 (2.079 Å)^[23] and KP1019 (2.061 Å).^[7b] An equatorial plane of four chloride ligands completes the coordination sphere with bond lengths ranging from 2.335–2.384 Å, which are within experimental error of KP418 (2.342–2.356 Å) and KP1019 (2.358–2.372 Å). This type of coordination environment is typical of analogous complexes.^[22]

Aqueous solution behavior: Due to the clinical success of KP1019, the solution behavior of this complex has been extensively studied by using a variety of techniques.^[11bd,13c,24] Aqueous exchange of a chloride ligand occurs within minutes under physiological conditions, resulting in the precipitation of the insoluble mono-aquated derivative.^[14a] This precipitation event can be inhibited in the presence of other ligands, particularly proteins or other biomolecules.^[11c,14a] For the compounds **1a–5a** and **1b–5b** reported here, we first characterized their ligand-exchange processes in phosphate-buffered saline (PBS, pH 7.4) to determine whether their fundamental solution behavior was similar to KP1019.

Because Ru^{III} is paramagnetic (low-spin d⁵, $S = 1/2$), EPR spectroscopy can be used to identify changes in the ligand environment around the metal center by analyzing the observed *g* values, the line widths, and the signal intensities. From these studies, species produced by ligand exchange can be identified, along with their rates of formation. Furthermore, processes that produce diamagnetic species, such as reduction to give Ru^{II} (low-spin d⁶, $S = 0$), can be monitored by a loss of the overall signal intensity due to the production of “EPR-silent” species. To track the solution behavior of the various Ru^{III} complexes, incubation under physiological conditions (pH 7.4, 37°C) was performed for up to 2 h, followed by freezing in liquid nitrogen after selected time points. EPR measurements of frozen solutions then provided a “snap-shot” of the paramagnetic species present at each time interval and their relative concentrations.

The ability of the Ru^{III} complexes **1a–5a** and **1b–5b** to undergo multiple ligand-exchange steps complicates the analysis of their EPR spectra by producing overlapping signals that require deconvolution. Spectral analyses were performed by simulating the spectra of each individual species present in solution, as defined by their *g* values and line widths. The spectrum from each spectral component was subsequently multiplied by a weighting factor, corresponding to the relative concentration of each Ru^{III} species present. The weighted spectra of each species identified were then summed together to reproduce the experimental data. To ensure that a unique solution was found for the spectral parameters of each species, only the weighting factors were varied between simulations of the EPR spectra at different incubation time points for each complex. We have previously demonstrated this approach in studies of KP1019, KP418,

and a number of other Ru^{III}-based anticancer drug candidates.^[14b,25]

Complexes **1a** and **1b** as well as **2a** and **2b** had sufficient aqueous solubility to be dissolved directly in PBS at a 3 mM concentration and studied by EPR spectroscopy. The other complexes, **3a–5a** and **3b–5b**, required the addition of 10% DMSO to give sufficient concentrations. Immediately after dissolution, similar uniaxial EPR spectra were observed for each of the parent Ru^{III} complexes, consistent with the tetragonal symmetry of the Ru^{III} centers prior to ligand exchange (**1b-C1** and **4a-C1** in Figure 3). Although the perpendicular part (g_{\perp}) of the EPR spectrum was well resolved in each case, g_{\parallel} could not be detected. A similar behavior has been reported in EPR measurements of KP1019 and KP418, and has been assigned to line broadening due to g strain.^[14b,26] In the earlier study of KP1019 and KP418, rapid-passage, dispersion-mode measurements determined $g_{\parallel}=1.20$ for both complexes. Given the structural and bonding similarity of the ruthenium centers with the compounds reported here, the value of g_{\parallel} is likely to be very similar. Thus, a value of $g_{\parallel}=1.20$ was used for the simulation of **1a–5a** and **1b–5b**, with a large line width (400 Gauss), but it should be noted that this has essentially no impact on the shape of the spectra in the perpendicular spectral region. Simulation of the perpendicular region gave values in the range $g_{\perp}=2.64–2.66$, and line widths of $LW_{\perp}=105–200$ Gauss (see Figures S1, S2, and S6–S15 as well as Tables S1 and S2 in the Supporting Information). The different counterions had no effect on the simulations for the spectra of complexes **1a** and **1b** as well as **2a** and **2b**. Similar EPR data was observed for complexes **3a** and **3b**, whereas for complexes **4a** and **3b** as well as **5a** and **5b**, the spectra from the pyridinium-compensated complexes were significantly broader than those with sodium ion compensation. This broadening is likely due to the highly hydrophobic nature of the pyridinium cations, leading to some aggregation of the complexes in solution.^[25a]

Incubation of 3 mM solutions of each complex in PBS at 37°C resulted in both precipitation and the formation of some soluble derivatives. We have previously used EPR spectroscopy to characterize ligand-exchange rates for both KP1019 and KP418.^[14b] In this work, we found rates of aqueous ligand exchange for the new pyridine analogues that are similar to KP1019. As expected, increasing the hydrophobicity of the axial ligands increased the rate of precipitation with incubation under physiological conditions. EPR measurements report primarily on the complexes in solution, because aggregation of precipitated compounds leads to spectral broadening. As a result, in these studies precipitation is reflected in a decrease in the overall EPR signal intensity with increasing incubation. For all of the complexes studied here, prolonged incubation was accompanied by a color change from clear yellow to dark green. In the case of complexes **3a–5a** and **3b–5b** significant amounts of a green-blue precipitate were also observed after longer incubation times. These observations are consistent with the formation of the mono-aqua derivatives, as reported for KP1019.^[14a,27]

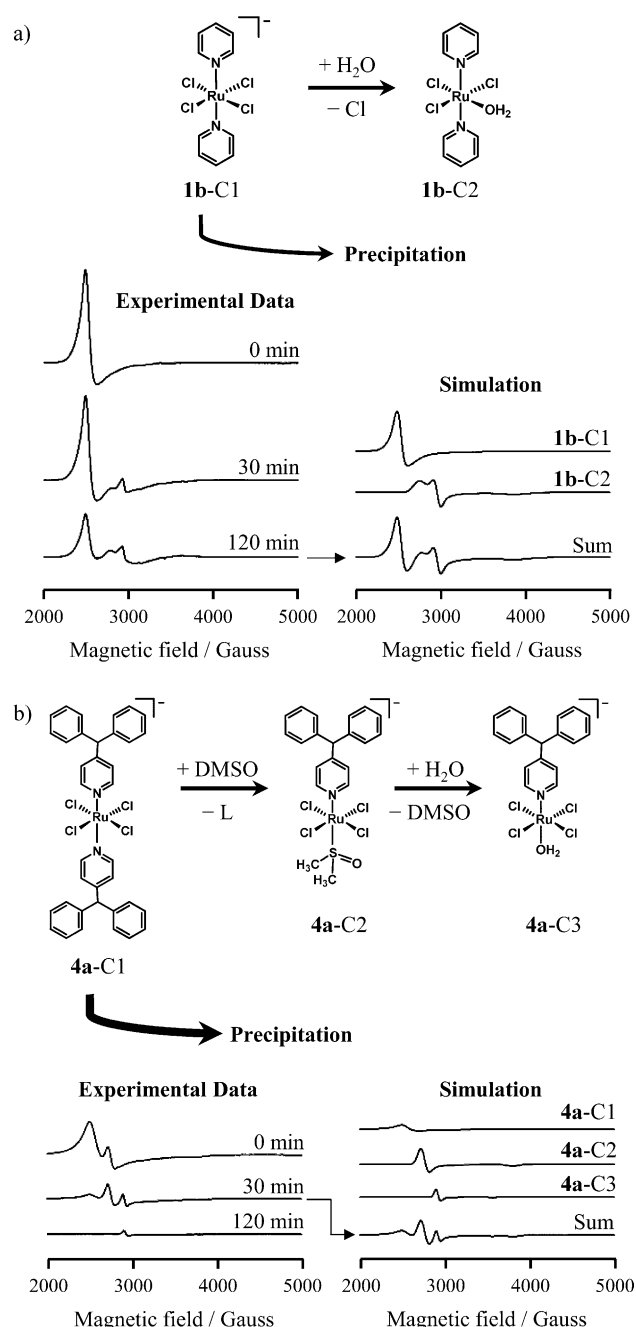


Figure 3. EPR measurements of: a) complex **1b** and b) complex **4a**, incubated in PBS at 37°C, and spectral deconvolution of spectra collected after 30 and 120 min of incubation. As shown by the spectral simulations, one new rhombic signal is observed for complex **1b** (**1b-C2**), whereas two axially symmetric species are observed for complex **4a** (**4a-C2** and **4a-C3**). Experimental parameters: frequency = 9.38 GHz, microwave power = 2.0 mW, time constant = 40.96 ms, modulation amplitude = 6 G, average of five two-minute scans. For EPR measurements of the solution behavior of the other complexes, see Figures S1 and S2 in the Supporting Information. For spectral deconvolution of spectra collected at each incubation time point for each complex, see Figures S6–S15 in the Supporting Information. For spectral parameters used in each simulation see Tables S1 and S2 in the Supporting Information.

To characterize the behavior of the complexes remaining in solution, EPR measurements were performed after incubation times of 0, 30, and 120 min. Spectral components

were analyzed by simulation, as described above and in the Experimental Section. In the case of complexes **1a** and **1b** a single new species was observed, which was identified by a rhombic EPR spectrum with $g=[2.44, 2.26, 1.72]$ and line widths of [130, 70, 300 Gauss], labeled **1b-C2** in Figure 3. This is consistent with the formation of the mono-aqua complex formed by the exchange of an equatorial chloride ligand. Similarly, for complexes **2a** and **2b**, only one new species was detected following dissolution. This was observed after 30 min of incubation: labeled **2a-C2** and **2b-C2** in Figures S8 and S9 in the Supporting Information with $g=[2.47/2.45, 2.27/2.26, 1.78/2.00]$ and line widths of [125, 100/50, 400 Gauss]. The similarity in the spectral parameters to complexes **1a-C1** and **1b-C1** indicates that these complexes also form a mono-aqua complex through chloride exchange.

Under physiological conditions nitrogen atom donor ligands are generally considered to be kinetically inert,^[28] leaving only the equatorial chloride ligands available for exchange with water molecules. To confirm this for complexes **1a** and **1b** as well as **2a** and **2b**, NMR measurements were made of the sodium-compensated complexes **1b** and **2b** in buffered D₂O solutions. These solutions were incubated at 37°C for 2 h and subsequently analyzed by using ¹H NMR spectroscopy to monitor the pyridine or 4-methylpyridine ligands, respectively (see Figures S61 and S62 in the Supporting Information). In both cases, no free pyridine-based ligands were observed, thereby confirming that only chloride ligand exchange occurs.

No soluble ligand-exchanged complexes were observed for the sodium-compensated complexes **3b-5b**. The more hydrophobic ligands of these compounds, as compared to complexes **1a** and **1b** as well as **2a** and **2b**, likely led to highly insoluble aquated derivatives, which precipitate rapidly and were thus not observed by EPR spectroscopy.

Although the pyridinium-compensated complexes **3a-5a** also precipitate readily, two new uniaxial EPR signals with relatively low intensity are observed. The first species to form ($g_{\perp}=2.44$, $g_{\parallel}=1.76$; $LW_{\perp}=90$ and $LW_{\parallel}=125$ Gauss) is labeled **4a-C2** in Figure 3 and correspondingly for complexes **3a** and **5a** in Figures S10 and S14 in the Supporting Information. With further incubation this was replaced by a second new species ($g_{\perp}=2.30$, $g_{\parallel}=1.88$; $LW_{\perp}=50$ and $LW_{\parallel}=50$ Gauss), identified as **4a-C3** in Figure 3 and similarly for the other complexes in the Supporting Information. Interestingly, the uniaxial EPR spectra for each species indicate tetragonal symmetry, which requires exchange of the pyridine-based ligands. To the best of our knowledge, this has not been reported previously for Keppler-type complexes under physiological conditions.

As described above, to achieve sufficient solubility for EPR measurements, DMSO was added to the solutions of **3a-5a** and **3b-5b**, a procedure that is also common in the preparation of these types of compounds for biological testing. The spectral parameters of the first species formed from complexes **3a-5a**, match those previously reported for "NAMI-A-type" pyridine complexes.^[25a,29] These complexes have the general formula [*trans*-RuCl₄(1*H*-L)(DMSO-*S*)],

where L is an axial pyridine-based ligand, DMSO takes up the opposite axial position, and charge compensation is provided by a pyridinium or sodium cation. Therefore, the first species to form, that is, C2, is assigned to exchange of an axial pyridine ligand for DMSO. The second type of species, that is, C3, which forms with longer incubation, has spectral parameters that match those of the NAMI-A-type complexes after the DMSO ligand had been exchanged for a water molecule, indicating that the same process is occurring here for complexes **3a-5a**.

As further evidence that this process involves exchange of a pyridine-based ligand for DMSO, we repeated the experiments with 50 and 100% DMSO. The signal from complexes **3a-C2-5a-C2**, was observed with increased intensity (see Figure S26 in the Supporting Information), which is consistent with the formation of the DMSO complex. ¹H NMR measurements could not be used in this case to detect exchanged pyridine-based ligands because their signals were masked by the pyridinium counterions, whereas the signal intensity was too low for paramagnetic NMR spectroscopy to detect coordinated DMSO molecules.

The replacement of pyridine ligands by DMSO is not unprecedented,^[30] but has not been reported for KP1019 under physiological conditions.^[2c] To confirm this, KP1019 was dissolved in PBS with 10% DMSO and measured by EPR spectroscopy (see Figure S58 in the Supporting Information). The resulting spectra are identical to those previously reported for the complex in DMSO-free buffer.^[11b,14b] Furthermore, with prolonged incubation at 37°C the EPR spectrum was unchanged and no precipitation occurred. This demonstrates that DMSO enhances the solubility of KP1019 by inhibiting the formation of the insoluble mono-aqua species, but does lead to an exchange of its indazole ligands.

The ligand-exchange processes of each compound were also characterized by UV/Vis spectroscopy. Samples were prepared in PBS at a concentration of 200 μM. Following the EPR experiments, solutions of complexes **3a-5a** and **3b-5b** included 10% DMSO. The samples were incubated at 37°C within the spectrophotometer with measurements taken every 10 min for two hours.

The UV/Vis spectra of complexes **1a** and **1b** (Figure 4 and Figures S27 and S28 in the Supporting Information) are essentially identical with absorption bands in both the ultraviolet and the visible range. The most intense peak is observed at $\lambda=257$ nm, and is assigned to the auxochrome signal from the pyridine ligand.^[31] The next most intense absorbance peak occurs at $\lambda=281$ nm, which is consistent with pyridine $\pi-\pi^*$ transitions for Ru^{III} complexes.^[32] A third peak at $\lambda=360$ nm is within the typical range of ligand-to-metal charge-transfer (LMCT) transitions for octahedral Ru^{III} complexes with bound nitrogen heterocycles.^[33] With incubation, the absorbances at $\lambda=257$ and 360 nm decrease, whereas the peak at $\lambda=281$ nm shifts slightly to longer wavelength. A well-defined isosbestic point ($\lambda=347$ nm) is observed, which is consistent with only one ligand-exchange pathway. This is in agreement with a single aquation step as determined by EPR spectroscopy, whereas the decrease in

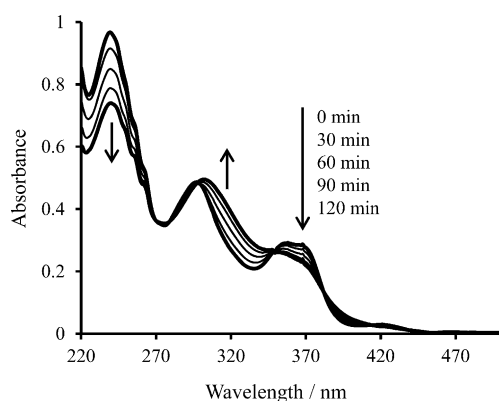


Figure 4. UV/Vis spectra for complex **1a** incubated in PBS for 2 h at 37°C.

the peak at $\lambda=257$ nm is consistent with the observed precipitation in the sample.

Similar absorbances and spectral changes with incubation were observed for complexes **2a** and **2b** (Figures S29 and S30 in the Supporting Information), which is consistent with a single aquation step, as also observed by EPR spectroscopy. Complexes **3a–5a** and **3b–5b** had spectra dominated by broad, intense features that did not change significantly with incubation (Figures S31–S36 in the Supporting Information). These absorbances are from $\pi-\pi^*$ transitions of the phenyl-based substituents. However, subtle changes in the signal intensities indicate ligand-exchange processes.

Overall, these studies demonstrate that aqueous solubility is a significant issue for all of these compounds, with precipitation occurring readily in buffered solutions. However, contributions from soluble mono-nuclear Ru^{III} species are also notable and there is some diversity in the mechanisms of their formation due to the different axial ligands.

Interactions of complexes with hsA: Human serum albumin is the most abundant protein in the circulatory system, and has been identified as a primary target in the transportation of many drugs to their sites of activity.^[34] Several studies have shown that hsA interactions are prevalent for Ru^{III} complexes under physiological conditions.^[11f,16,35] The propensity of albumin to form interactions with a variety of pharmaceuticals has been reported^[36] and is considered to be an important factor in their delivery to their sites of action. Indeed, the use of albumin in drug delivery has developed into a promising area of medicinal chemistry.^[37] However, the majority of the uses of albumin rely on coordinate interactions between the pharmaceutical and the protein.^[38] Here, we focus on optimizing non-coordinate hsA interactions, in part to reduce coordination to the protein and thereby increase the bioavailability of the complex.

We have previously used EPR methods to show that KP1019 forms rapid non-coordinate interactions with hsA,^[14b] which are gradually converted to coordinate protein interactions after further incubation under physiological conditions. In the case of its toxic imidazole analogue

(KP418), non-coordinate protein interactions are also observed, however, they form at a much slower rate.^[14b,20] The reduced rate of hsA binding by KP418 has been suggested to leave more of the complex free in vivo, and is possibly responsible for its observed toxicity.^[39] In light of these reports, we have studied the ability of complexes **1a–5a** and **1b–5b** to bind to hsA, both through hydrophobic interactions and through direct coordination.

The complexes **1a–5a** and **1b–5b** were incubated for 0 and 30 min as well as 1, 2, 6, and 24 h at 37°C in solutions of hsA in PBS. Protein-bound fractions were then isolated by using centrifugal ultrafiltration and studied by EPR spectroscopy. This approach allows us to observe exclusively hsA-bound Ru^{III} species while removing contributions from free complexes in solution.^[14b,25] The resulting spectra for select incubation times are shown in Figure 5 for complexes **1a**, **3a**, and **5a**, and in the Supporting Information (Figures S3–S5) for the other complexes at all time points.

After incubation with hsA, spectra from the unsubstituted parent compounds of each complex were observed even at the earliest time point (labeled “0 min” in Figure 5). This was confirmed by spectral simulation by using the parameters determined from the complexes dissolved directly in buffer, and identified previously as species C1. Because these measurements are of isolated protein fractions, they demonstrate that each complex readily binds to hsA without exchanging ligands, indicating non-coordinate interactions with the protein. Furthermore, the EPR spectra of the pyridinium-compensated compounds **4a** and **5a** exhibited narrower line widths than in buffer alone (labeled “**4a**-C1-hsA” and “**5a**-C1-hsA” in Figures S22 and S24 in the Supporting Information), indicating that protein interactions improve the solubility of the complexes.

Aquated derivatives of the complexes **1a** and **1b** as well as **2a** and **2b** were also observed to form non-coordinate interactions with hsA (see Figures S16–S19 in the Supporting Information). Simulation of the EPR spectra from these species gave parameters that agreed within experimental uncertainty with the corresponding compounds in buffer alone. For complexes **3a** as well as **4a** and **4b** the NAMI-A-type complexes formed by axial ligand exchange were again observed as minor contributors in the experimental spectrum (see Figures S20, S22, and S23 in the Supporting Information), whereas only the parent complex for complexes **3b**, **5a**, and **5b** was visible (see Figures S24 and S25 in the Supporting Information), demonstrating the influence of protein interactions on ligand-exchange processes. In previous studies, we have also observed aquated derivatives of KP418 and NAMI-A interacting with hsA.^[14b,25b]

Further incubation of each complex with hsA resulted in a gradual decrease in the signals from the parent compounds and their exchanged derivatives, coupled with the appearance of new broad features in their EPR spectra. Spectral simulations revealed two new signals in all cases, with relative intensities and formation rates that varied for each complex. The first new species, labeled “hsA-1” in Figure 5 (see Figures S16–S25 in the Supporting Information for each

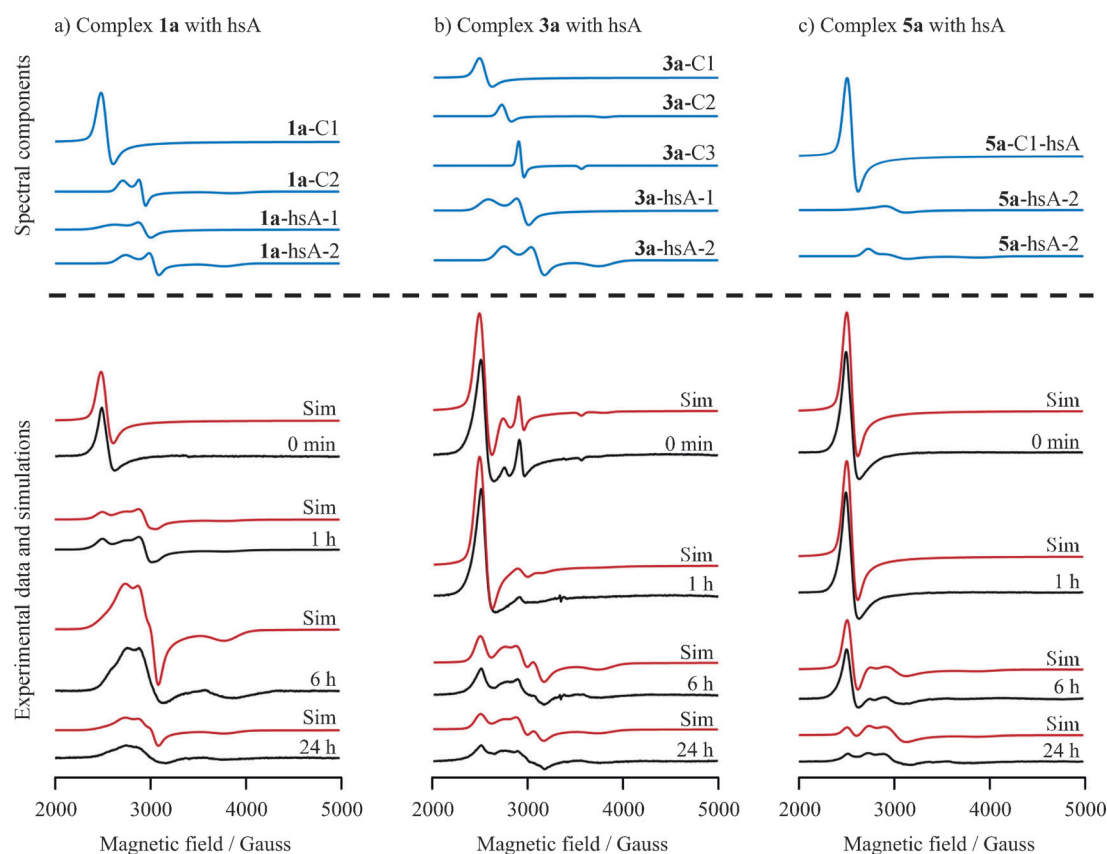


Figure 5. EPR measurements of complexes a) **1a**, b) **3a**, and c) **5a** incubated in PBS (1 mM, and 4% DMSO for complexes **3a** and **5a**) with hsA (0.5 mM) at 37°C, and spectral deconvolution of all spectra collected (shown in red) from the individual components (top of each column). Experimental parameters: frequency = 9.38 GHz, microwave power = 2.0 mW, time constant = 40.96 ms, modulation amplitude = 6 G, average of five two-minute scans. For EPR measurements of the hsA binding behavior of the other complexes, see the Supporting Information, Figures S3–S5. For spectral deconvolution of spectra collected at each incubation time point for each complex, see the Supporting Information, Figures S16–S25. For spectral parameters used in each simulation see the Supporting Information Tables S1 and S2.

complex), has a rhombic spectrum with $g_1 = 2.38\text{--}2.61$, $g_2 = 2.24\text{--}2.29$, and $g_3 = 1.20$, and line widths of: [$LW_1 = 175\text{--}400$, $LW_2 = 100\text{--}150$, and $LW_3 = 400$ Gauss]. The second species also has a rhombic EPR signal, labeled “hsA-2” in Figure 5, with $g_1 = 2.38\text{--}2.45$, $g_2 = 2.16\text{--}2.22$, and $g_3 = 1.71\text{--}1.78$, and line widths of: [$LW_1 = 80\text{--}150$, $LW_2 = 80\text{--}200$, and $LW_3 = 250\text{--}300$ Gauss] (see Tables S1 and S2 in the Supporting Information for parameters for each complex). In each case, the distinctive g values and line widths of these species are consistent with direct coordination to hsA through ligand exchange. Histidine coordination has previously been implicated in the protein binding of KP1019^[17,40] and other Ru^{III} complexes,^[2d,25b,41] and is expected to be the coordination mode seen here. The rhombic EPR spectra observed are consistent with coordination at equatorial positions, whereas the presence of two distinct signals indicates concurrent aquation processes. Given that hsA-1 has a greater signal intensity, particularly at early time points, this is likely the species formed by a single exchange with a histidine imidazole. Subsequent aqueous exchange likely then produces the second protein-bound species hsA-2.

Previous studies of Ru^{III}-based anticancer candidates have reported the coordination of upwards of five equivalents of

Ru per protein molecule.^[17,18] In this work we used a 2:1 ratio of each complex to hsA, to allow for the possibility of different binding modes. Strong signals from hsA-1 and hsA-2 were observed for every complex, demonstrating that protein coordination is highly favored and that the ruthenium center remains in the 3+ oxidation state. Furthermore, the signal intensity from the coordinated species was maintained even after 24 h of incubation, demonstrating how effectively these interactions stabilize the compounds in solution. A similar behavior has been reported previously for KP1019.^[11b,14]

To determine the effect of the different axial ligands of complexes **1a–5a** and **1b–5b** on interactions with hsA, spectra of each complex were collected at different incubation time points and analyzed by simulation (see Figures S16–S25 in the Supporting Information). From this analysis the relative total signal intensities from non-coordinate and coordinate interactions could be determined from the weighting factors used to scale individual spectral components in each simulation. Every complex showed significant non-coordinate interactions with hsA after minimal incubation times. However, the rate that these species were replaced by protein-coordinated complexes varied dramatically

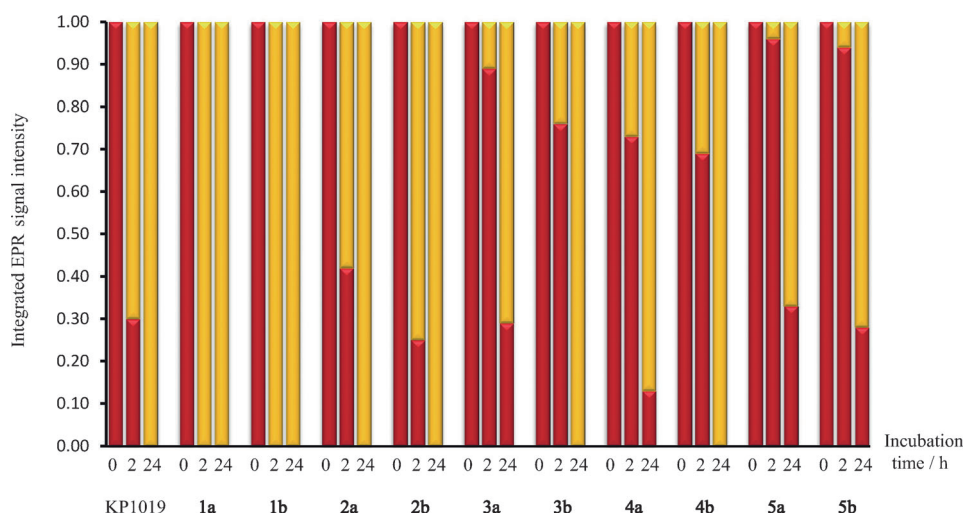


Figure 6. Relative fractions of coordinate (yellow) and non-coordinate (red) hsA-bound Ru^{III} complexes following 0, 2, and 24 h of incubation at 37°C, as determined by simulation of the EPR spectra.

(Figure 6). In the case of the unsubstituted pyridine complexes **1a** and **1b**, this process was complete after just 2 h of incubation, with only the protein-bound species hsA-1 and hsA-2 observed with subsequent incubation. A similar behavior was observed for complexes **2a** and **2b**, except that it took up to 6 h of incubation until non-coordinate species were no longer observed. This demonstrates that the methyl group at the 4'-position of the pyridine rings significantly enhances these interactions with the protein. This effect is even more pronounced in the complexes where the pyridine ligands have been functionalized with phenyl-based groups. In the case of complexes **3a** and **3b** significant contributions from non-coordinated species were observed after 6 h of incubation, and even after 24 h for the pyridinium-compensated compound. The protein binding of complexes **4a** and **4b** was very similar to the mono-phenyl derivatives, demonstrating that addition of the second phenyl ring does not significantly enhance non-coordinate interactions. Specific interactions with the hydrophobic binding regions, that is, the Sudlow's sites I and II of hsA,^[19] have previously been suggested as targets for interactions with Keppler-type complexes.^[14a,18c] Although increasingly hydrophobic groups would certainly be expected to enhance interactions with these protein sites, such as observed in the trend in the binding of complexes **1a–3a** and **1b–3b**, steric interactions, such as from the bulky dibenzyl groups of complexes **4a** and **4b** are likely also to be an important factor.

Interestingly, the most stabilized non-coordinate interactions are provided by the nitrobenzyl-functionalized compounds **5a** and **5b**. Even after 24 h of incubation, significant signals from non-coordinated species were observed, and the rate of coordination to hsA was lower than any of the other compounds. Spectral simulation determined that the non-coordinate signal for complex **5a** was the largest, accounting for roughly 33% of the observed EPR intensity (Figure 6). Comparison with complexes **3a** and **3b** is particularly relevant because it demonstrates the importance of

the nitro groups. Increased stabilization of hydrophobic binding due to electrostatic interactions imparted by this functionality is in agreement with the observation that hsA has a high affinity for anionic species.^[42] Overall, non-coordinate binding to hsA was more prolonged for the pyridinium compensated complexes, as compared to the sodium compensated complexes, likely reflecting their aqueous insolubility, thereby promoting interactions with the hydrophobic regions of hsA, and inhibiting ligand exchange.

UV/Vis measurements were also used to characterize the interactions of the complexes

with hsA. Each compound (200 μM) was incubated with the protein (100 μM) at 37°C in PBS and monitored for up to 2 h; 4% DMSO were added to solutions of complexes **3a–5a** and **3b–5b** to aid in solubility. The time dependence of the UV/Vis measurements is shown in Figures S37–S46 in the Supporting Information for all of the compounds. During the first 2 h of incubation, the spectra do not differ significantly from those observed in the absence of the protein, indicating similar species in solution. This is consistent with the EPR observations of the parent compounds of **1a–5a** and **1b–5b** and their aquated derivatives interacting with hsA through non-coordinate interactions, and may also reflect a fraction of complexes that remain free in solution.

Additional samples were prepared of each complex (600 μM) with hsA (100 μM) to monitor for a weak d–d transition at high wavelengths associated with coordinate hsA interactions.^[43] Because the EPR experiments demonstrated that such interactions only dominate after prolonged incubation, the samples were measured for up to 24 h at 37°C. For each complex, broadening of the spectra and the appearance of a low intensity band at λ = 625–657 nm was observed (Figure 7 for complex **1a**, 24-hour spectra for all complexes are shown in Figures S47–S56 in the Supporting Information). A similar feature at λ = 575 nm has been reported following incubation of KP1019 with hsA^[18a] and is also observed for KP1019 under the conditions used in our experiments (see Figure S60 in the Supporting Information). This absorbance has been proposed to arise from a d–d transition that is specific for hsA coordination to a surface histidine.^[17] The assignment of this transition for complexes **1a–5a** and **1b–5b** and the rate that its intensity increases with incubation are in agreement with the EPR results indicating formation of coordinate interactions of the complexes with hsA.

The observation of ligand-dependent stabilization of non-coordinate interactions with hsA has important implications for drug design. The coordination of KP1019 to hsA has

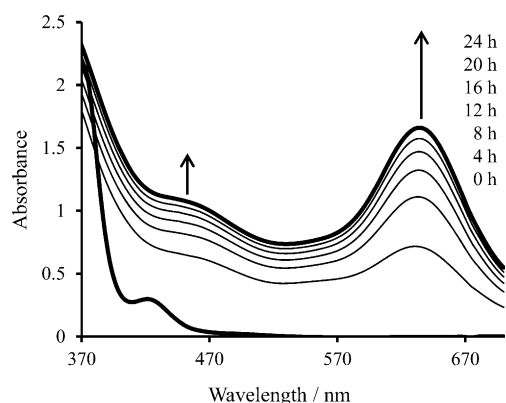


Figure 7. UV/Vis spectra for complex **1a** incubated with hsA for 24 h at 37°C.

been suggested to potentially impact on its observed anticancer activity.^[11c] As we have demonstrated here, enhancement of non-coordinate interactions with hydrophobic ligands, possibly with the addition of polarized groups, can inhibit the formation of coordinated species. This design strategy has the potential to increase the concentration of the active species in vivo.

As we have shown, non-coordinate interactions with hsA also enhance the solubility of these complexes. This suggests that preparation of the compounds with hsA prior to intravenous administration could help to stabilize them in solution while also increasing the concentrations of active species. In essence, such an approach can be considered as the application of non-coordinate protein conjugates. To test the viability of this approach, the anticancer activity of the new compounds described here was evaluated with and without prior incubation with hsA.

Biological activity: Anticancer activity screening was performed against the SW480 human colorectal cancer cell line. This cell line was chosen to allow for comparison with previous studies of KP1019 and KP1339.^[8a,d,11a] In these studies, the maximum concentrations used in testing of the free complexes varied due to differences in their aqueous solubility. This issue was significant enough to prevent meaningful testing of the pyridinium-compensated complexes **3a–5a**. However, all the remaining compounds, that is, complexes **1a** and **2a** as well as **1b–5b** were subjected to in vitro studies. To probe the effect of hsA interactions on the activity of the compounds, two sets of experiments were performed: 1) the compounds were dissolved in cell culture medium with 1% DMSO and then incubated with the SW480 cells for 24 h, and 2) the compounds were dissolved in PBS with 1% DMSO and incubated with hsA for one hour at room temperature, after which the protein-bound fractions were isolated and tested, as described in the Experimental Section.

Screening of the free complexes revealed that they were relatively inactive against the SW480 cell line. Complex **2b** (Figure 8) and **2a** (Figure S63 in the Supporting Informa-

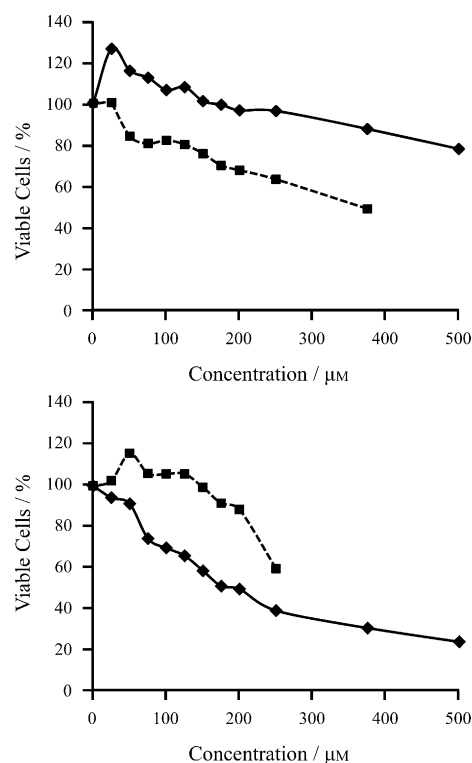


Figure 8. MTS assay results for complexes **2b** (top) and **4b** (bottom). ■ = free complex in solution and ◆ = complex pre-incubated with hsA.

tion) had IC₅₀ values of approximately 400 μM, whereas the other pyridine-based complexes **1a**, **1b** and **3b–5b** were inactive at their maximum concentrations (Figures 8 and S63 in the Supporting Information). Pre-incubation of the compounds with hsA had notable effects on the activity of the methyl- (i.e., complexes **2a** and **2b**) and dibenzyl-substituted (i.e., complex **4b**) complexes. In the case of complexes **2a** and **2b** a decrease in activity was observed following incubation with hsA (Figures 8 and S63 in the Supporting Information). This observation is consistent with coordination of the complexes to the protein, which potentially reduces their bioavailability. By contrast, pre-incubation of complex **4b** with hsA resulted in an increased activity. In fact, this preparation provided the most activity of any of the tests with an IC₅₀ value of approximately 150 μM (Figure 8). This is particularly striking given the inactivity of the free complex. The observed increase in activity is possibly related to the stabilized hydrophobic interactions with hsA observed for complex **4b**, which may enhance the bioavailability of the complex through inhibition of protein coordination.

The low activity of the pyridine-based compounds in this report is consistent with previous in vitro cell studies of Keppler-type complexes.^[8a,22a,44] However, several studies have shown that the low intrinsic cytotoxicity predicted in such studies frequently underestimates the in vivo activity of these types of compounds, which have shown excellent anti-tumor properties in several studies.^[7a,8c,45] A key example of this is the sodium-compensated bisindazole complex KP1339 (Figure 1), which is currently undergoing clinical trials,^[8e,10]

and yet only shows an IC_{50} of $120\ \mu\text{M}$ against the SW480 cell line.^[8a] This is similar to the best result for our compounds, which was an IC_{50} of approximately $150\ \mu\text{M}$ for compound **4b** after incubation with hsA. We note also that the activity of complex **4b** with hsA is higher than that of KP1019 with or without incubation with hsA under the testing conditions used here (Figure S63 in the Supporting Information). With such low intrinsic cytotoxicity, the *in vivo* activity^[8a,d,18b] and clinical success of KP1019 and KP1339 are due in part to the very low levels of side effects they exhibit.^[2b,8b] This allows for high concentrations of the compounds to be used during treatments.^[2a,b]

It should be emphasized that the design of compounds **1a–5a** and **1b–5b** was primarily to target protein interactions for comparative studies, rather than activity specifically. The use of non-coordinate hsA conjugates has been explored with conventional organic anticancer compounds, in some cases resulting in improved activity.^[46] However, this is the first such study for Ru^{III}-based bisazole complexes. Indeed, despite successful clinical trials for both KP1019 and KP1339, relatively few derivatives of these compounds have been reported.^[7a,21,22,47]

Another useful consequence of incubating complexes **1a–5a** and **1b–5b** with hsA was the improved solubility. This is a particularly important observation given the low intrinsic cytotoxicity of Keppler-type complexes described above. In the studies reported here, the compounds were dissolved in culture media and then added to an equal volume of cells and media, which reduced the testing concentration by a factor of two. Thus, for the highest concentration solutions used in testing, that is, $500\ \mu\text{M}$, an initial solution with a concentration of $1\ \text{mM}$ was required. At this concentration, precipitation was significant for compounds **3b–5b**, which could only be prepared in concentrations of half this value or less. However, if the complexes were first incubated with hsA they all could be prepared at the maximum concentration without precipitation. As shown in Figure 8, incubation of compound **4b** with hsA increases the maximum testing concentration from $250\ \mu\text{M}$ to at least $500\ \mu\text{M}$. This suggests an advantage in preparing these types of compounds with hsA for clinical studies by preventing precipitation and allowing for higher concentrations for treatment solutions.

Conclusion

For Keppler-type Ru^{III}-based anticancer complexes, two key aspects of their prodrug behavior are aqueous ligand exchange, and serum–protein interactions. This can lead to a variety of species in solution, which may inhibit or promote their activity. As shown here, hydrophobic interactions with albumin can potentially enhance the concentration of active species *in vitro*. At the most fundamental level, this is from increased solubilization of the complexes in aqueous solution through inhibition of precipitation. This suggests that the preparation of these complexes for intravenous therapy with hsA could be advantageous for stabilizing the

active species prior to treatment. Although DMSO has traditionally been used for this purpose, as we have shown here, this can potentially influence ligand-exchange processes by coordination of DMSO through replacement of an azole ligand. Such processes are expected to reduce the cytotoxicity of the compounds by producing species analogous to NAMI-A-type complexes.

Because the origin of the anticancer activity of Keppler-type complexes remains unknown, the effect of modifications to their axial azole ligands continues to be hard to rationalize. In this work we have been able to show how these ligands can influence interactions with hsA, and how this correlates with the hydrophobic properties of their substituents. Although the predicted stabilization of non-coordinate protein interactions generally correlates with the hydrophobic properties of the ligands, closer analysis indicates that other factors are also important. The observation that the dibenzyl complex does not provide the anticipated increase in non-coordinate interactions over the benzyl-substituted compound suggests that steric factors should also be considered. Furthermore, the remarkable stability of non-coordinate interactions with the nitrobenzyl compounds suggests that polarizable substituents could increase the interactions with the binding sites, possibly through hydrogen bonding.

Generally, the pyridine-based analogues of KP1019/KP1339 were relative inactive against the SW480 cell line. However, results from complexes **2a**, **2b**, and **4a** do provide some insight into the effects of hsA because the former show a decrease in activity in the presence of the protein, whereas the later shows an increase. This correlates with our determination of a greater proportion of coordinate interactions of complexes **2a** and **2b** with hsA and more non-coordinate interactions for complex **4b**. In the case of compound **4b** this suggests greater bioavailability, and is particularly notable because it is inactive as the free complex, but after pre-treatment with hsA exhibits activity similar to the clinically successful compound KP1339.^[8e,10] Overall, these results suggest that targeting of non-coordinate interactions with hsA could be a promising direction in the on-going development of Keppler-type Ru^{III}-based anticancer complexes.

Experimental Section

Materials: The starting compounds RuCl₃·H₂O (Aldrich), pyridine (Anachemia), 4-methylpyridine (TCI America), 4-phenylpyridine (Aldrich), diphenyl-4-pyridyl-methane (Aldrich), and 4-(4-nitrobenzyl)pyridine (Alfa Aesar) as well as human serum albumin (Aldrich) were used as purchased.

Crystallographic structure determination: Single-crystal X-ray crystallographic analysis was performed on a Bruker SMART diffractometer equipped with an APEX II CCD area detector fixed at a distance of 6.0 cm from the crystal and a MoK α fine focus sealed tube ($\lambda = 0.71073\ \text{nm}$) operating at 1.5 kW (50 kV, 30 mA) and filtered with a graphite monochromator. Structures were solved by using direct methods (SIR92) and refined by least-squares procedures in CRYSTALS.^[48] Diagrams of complexes **1a**, **2a**, **3b**, **4a**, and **5a** were generated by ORTEP-3 for Windows (v. 2.00).^[49] Crystal data, data collection param-

ters, and details of structure refinement for compounds **1a**, **2a**, **3b**, **4a**, and **5a** are listed in Table S3 in the Supporting Information.

CCDC-968766 (**1a**), CCDC-968767 (**2a**), CCDC-968768 (**3b**), CCDC-968769 (**4a**) and CCDC-968770 (**5a**) contain the supplementary crystallographic data for this paper. These data can be obtained free of charge from The Cambridge Crystallographic Data Centre via www.ccdc.cam.ac.uk/data_request/cif.

Optical measurements: UV/Vis spectra were measured by using a Cary 1E UV-Visible spectrophotometer, connected to a Haake F3 water bath, which maintained the temperature of each sample at 37°C. Spectra were collected from samples dissolved in a PBS solution containing: NaCl (137 mM), KCl (2.7 mM), Na₂HPO₄ (10 mM), and KH₂PO₄ (2 mM), pH 7.4, with complexes **3a–5a** and **3b–5b** having 10% DMSO added to aid in solubility. Measurements were performed by using 200 µM solutions of each complex in 1 mL volumes. Protein binding measurements were performed by using 200 µM solutions of each complex and 100 µM hsA in 1 mL volumes, with 4% DMSO added to the solutions of complexes **3a–5a** and **3b–5b**. All samples were measured at 37°C for a total of 2 h, with scans taken at 10 min intervals, at a scan rate of 10 nm s⁻¹. Additional protein samples were prepared to monitor for a weak d–d transition corresponding to hsA coordination by using a 600 µM concentration of each complex and a 100 µM concentration of hsA. These samples were incubated at 37°C for 24 h with one hour scan intervals.

Preparation of EPR samples

Complexes in buffer: Compounds were dissolved in PBS with complexes **3a–5a** and **3b–5b** having 10% DMSO added to aid in solubility, to give a concentration of 3 mM, and incubated at 37°C for 0, 30, and 120 min. Each sample was promptly mixed with 30% by volume of glycerol, which acted as a glassing agent, and frozen in liquid nitrogen until use.

Complexes with hsA: A solution of hsA (600 µL, 0.75 mM) in PBS was mixed with a 600 µL solution of each complex (1.5 mM), also in PBS with complexes **3a–5a** and **3b–5b** having 4% DMSO added to aid in solubility. The combined solution was then diluted to 4 mL with PBS and incubated at 37°C for one of the following time periods: 0, 30 min, 1, 2, 6, and 24 h. Each 4 mL solution was concentrated down to a volume of less than 200 µL by using an Amicon centrifugal filter unit (molecular weight cut-off 30 kDa) by centrifuging at 8°C and 4500 rpm for 30 min, or until a volume of less than 200 µL was attained. The resulting filtered product was then mixed with 90 µL of glycerol, diluted to a final volume of 300 µL with PBS, transferred to an EPR tube, and immediately frozen in liquid nitrogen.

EPR measurements and simulations: EPR measurements were performed at X-band (9.3–9.4 GHz) by using a Bruker EMXplus spectrometer with a PremiumX microwave bridge and HS resonator. Low-temperature (20 K) experiments used a Bruker ER 4112HV helium temperature-control system and continuous-flow cryostat. Solution conditions and spectroscopic parameters were unchanged for each experiment so that the intensities of the EPR signals from Ru^{III}-based species in different samples could be compared. The Bruker cryostat system contains a quartz-insert tube holder that enables reproducible sample placement within the EPR resonator. Consequently, variation in instrument sensitivity between measurements was minimal, and automatic tuning of the spectrometer gave a Q-factor of (7000 ± 10)%. In experiments with hsA, the distinctive EPR signal from a minor Fe^{III} human serum transferrin impurity at g = 4.3 also provided a reference for normalizing the Ru^{III} EPR signal sensitivity.

All spectra were simulated by using the program WinEPR Simfonia,^[50] which efficiently produces accurate results for S = 1/2 systems. A manual, iterative fitting procedure was employed to analyze the overlapping spectra from multiple Ru^{III} species observed in many samples.

Anticancer activity testing: Complexes were tested for anticancer activity by using a standard MTS (3-(4,5-Dimethylthiazol-2-yl)-5-(3-carboxymethoxyphenyl)-2-(4-sulfophenyl)-2H-tetrazolium) assay (Promega). SW480 human colon carcinoma cells were obtained from the American Type Culture Collection (ATCC). The cells were cultured by using Dulbecco's modified eagle medium (DMEM), supplemented with 10% fetal bovine serum (FBS), and l-glutamine. Fresh stock solutions of each free complex

were prepared in cell culture media with 1% DMSO, at the maximum concentration possible for each complex: 1 mM for complexes **1a**, **1b**, **2a**, and **2b**, 500 µM for complexes **3b** and **4b**, and 750 µM for complex **5b**. Due to their low aqueous solubility, complexes **3a**, **4a**, and **5a** were not tested. Cells were incubated with each complex for 24 h, after which the absorbance reading at λ = 490 nm was measured as an indicator of activity.

Additional samples were prepared where the complexes were loaded onto hsA. Solutions of each complex in PBS (1 mM, 1% DMSO) were mixed with solutions of hsA in PBS (0.5 mM) and incubated for 10 min at 37°C, after which the protein-bound fractions were isolated, as described above for the preparation of the EPR samples. The fractions were then incubated at room temperature for one hour prior to being diluted in cell culture medium and subsequently tested for activity by using identical conditions as for the free complexes.

Acknowledgements

The authors are grateful for the financial support of The Natural Sciences and Engineering Research Council of Canada (NSERC): C.J.W. for NSERC Discovery Grant funding, and M.I.W. for an NSERC postgraduate doctoral scholarship (PGS-D). The Canada Foundation for Innovation (CFI), and Simon Fraser University are also acknowledged.

- [1] a) A. Bergamo, G. Sava, *Dalton Trans.* **2011**, 40, 7817–7823; b) A. Bergamo, C. Gaiddon, J. H. M. Schellens, J. H. Beijnen, G. Sava, *J. Inorg. Biochem.* **2012**, 106, 90–99.
- [2] a) C. G. Hartinger, M. A. Jakupec, S. Zorbas-Seifried, M. Groessl, A. Egger, W. Berger, H. Zorbas, P. J. Dyson, B. K. Keppler, *Chem. Biodiversity* **2008**, 5, 2140–2155; b) F. Lentz, A. Drescher, A. Lindauer, M. Henke, R. A. Hilger, C. G. Hartinger, M. E. Scheulen, C. Dittrich, B. K. Keppler, U. Jaehde, *Anti-Cancer Drugs* **2009**, 20, 97–103; c) R. E. Aird, J. Cummings, A. A. Ritchie, M. Muir, R. E. Morris, H. Chen, P. J. Sadler, D. I. Jodrell, *Br. J. Cancer* **2002**, 86, 1652–1657; d) A. Bergamo, A. Masi, P. J. Dyson, G. Sava, *Int. J. Oncol.* **2008**, 33, 1281–1289; e) J. M. Rademaker-Lakhai, D. van den Bongard, D. Pluim, J. H. Beijnen, J. H. M. Schellens, *Clin. Cancer Res.* **2004**, 10, 3717–3727.
- [3] a) J. Reedijk, *Platinum Met. Rev.* **2008**, 52, 2–11; b) S. Page *Educ. Chem.* **2012**, 49, 26–29.
- [4] C. S. Allardyce, P. J. Dyson, *Platinum Met. Rev.* **2001**, 45, 62–69.
- [5] a) M. A. Jakupec, M. Galanski, V. B. Arion, C. G. Hartinger, B. K. Keppler, *Dalton Trans.* **2008**, 183–194; b) E. Alessio, G. Mestroni, A. Bergamo, G. Sava, *Curr. Top. Med. Chem.* **2004**, 4, 1525–1535; c) G. Gasser, I. Ott, N. Metzler-Nolte, *J. Med. Chem.* **2011**, 54, 3–25.
- [6] A. Levina, A. Mitra, P. A. Lay, *Metallomics* **2009**, 1, 458–470.
- [7] a) K.-G. Lipponer, E. Vogel, B. K. Keppler, *Met.-Based Drugs* **1996**, 3, 243–260; b) W. Peti, T. Pieper, M. Sommer, B. K. Keppler, G. Giester, *Eur. J. Inorg. Chem.* **1999**, 1551–1555.
- [8] a) S. Kapitzka, M. Pongratz, M. A. Jakupec, P. Heffeter, W. Berger, L. Lackinger, B. K. Keppler, B. Marian, *J. Cancer Res. Clin. Oncol.* **2005**, 131, 101–110; b) C. G. Hartinger, S. Zorbas-Seifried, M. A. Jakupec, B. Kynast, H. Zorbas, B. K. Keppler, *J. Inorg. Biochem.* **2006**, 100, 891–904; c) M. H. Seelig, M. R. Berger, B. K. Keppler, D. Schmahl in *Metal Ions in Biology and Medicine*, French & European Publications, New York, **1990**, pp. 476–478; d) S. Kapitzka, M. A. Jakupec, M. Uhl, B. K. Keppler, B. Marian, *Cancer Lett.* **2005**, 226, 115–121; e) M. M. Henke, H. Richly, A. Drescher, M. Grubert, D. Alex, D. Thyssen, U. Jaehde, M. E. Scheulen, R. A. Hilger, *Int. J. Clin. Pharmacol. Ther.* **2009**, 47, 58–60.
- [9] J. B. Aitken, S. Antony, C. M. Weekley, B. Lai, L. Spiccia, H. H. Harris, *Metallomics* **2012**, 4, 1051–1056.
- [10] R. Trondl, P. Heffeter, M. A. Jakupec, W. Berger, B. K. Keppler, *BMC Pharmacol. Toxicol.* **2012**, 13, A82.

- [11] a) P. Heffeter, K. Bock, B. Atil, M. A. R. Hoda, W. Korner, C. Bartel, U. Jungwirth, B. K. Keppler, M. Micksche, W. Berger, G. Koellensperger, *J. Biol. Inorg. Chem.* **2010**, *15*, 737–748; b) A. Kung, T. Pieper, R. Wissiack, E. Rosenberg, B. K. Keppler, *J. Biol. Inorg. Chem.* **2001**, *6*, 292–299; c) K. Poleć-Pawlak, J. K. Abramski, J. Ferenc, L. S. Foteeva, A. R. Timerbaev, B. K. Keppler, M. Jarosz, *J. Chromatogr. A* **2008**, *1192*, 323–326; d) J. C. Chen, L. M. Chen, S. Y. Liao, K. Zheng, L. N. Ji, *Dalton Trans.* **2007**, 3507–3515; e) M. Groessl, C. G. Hartinger, P. J. Dyson, B. K. Keppler, *J. Inorg. Biochem.* **2008**, *102*, 1060–1065; f) M. Groessl, C. G. Hartinger, A. Egger, B. K. Keppler, *Met. Ions Biol. Med.* **2006**, *9*, 111–116; g) A. Levina, J. B. Aitken, Y. Y. Gwee, Z. J. Lim, M. Liu, A. M. Singharay, P. F. Wong, P. A. Lay, *Chem. Eur. J.* **2013**, *19*, 3609–3619; h) A. A. Hummer, P. Heffeter, W. Berger, M. Filipits, D. Batchelor, G. E. Buchel, M. A. Jakupec, B. K. Keppler, A. Rompel, *J. Med. Chem.* **2013**, *56*, 1182–1196.
- [12] C. Anderson, A. L. Beauchamp, *Can. J. Chem.* **1995**, *73*, 471–482.
- [13] a) G. Sava, A. Bergamo, S. Zorzet, B. Gava, C. Casarsa, M. Cocchietto, A. Furlani, V. Scarcia, B. Serli, E. Iengo, E. Alessio, G. Mestroni, *Eur. J. Cancer* **2002**, *38*, 427–435; b) M. Groessl, E. Reisner, C. G. Hartinger, R. Eichinger, O. Semenova, A. R. Timerbaev, M. A. Jakupec, V. B. Arion, B. K. Keppler, *J. Med. Chem.* **2007**, *50*, 2185–2193; c) T. Pieper, W. Peti, B. K. Keppler, *Met.-Based Drugs* **2000**, *7*, 225–232.
- [14] a) F. Kratz, M. Hartmann, B. Keppler, L. Messori, *J. Biol. Chem.* **1994**, *269*, 2581–2588; b) N. Cetinbas, M. I. Webb, J. A. Dubland, C. J. Walsby, *J. Biol. Inorg. Chem.* **2010**, *15*, 131–145.
- [15] A. R. Timerbaev, C. G. Hartinger, S. S. Aleksenko, B. K. Keppler, *Chem. Rev.* **2006**, *106*, 2224–2248.
- [16] C. G. Hartinger, S. Hann, G. Koellensperger, M. Sulyok, M. Groessl, A. R. Timerbaev, A. V. Rudnev, G. Stinger, B. K. Keppler, *Int. J. Clin. Pharmacol. Ther.* **2005**, *43*, 583–585.
- [17] F. Piccioli, S. Sabatini, L. Messori, P. Orioli, C. G. Hartinger, B. K. Keppler, *J. Inorg. Biochem.* **2004**, *98*, 1135–1142.
- [18] a) L. Trynda-Lemiesz, A. Karaczyn, B. K. Keppler, H. Kozłowski, *J. Inorg. Biochem.* **2000**, *78*, 341–346; b) A. K. Bytzeck, K. Boeck, G. Hermann, S. Hann, B. K. Keppler, C. G. Hartinger, G. Koellensperger, *Metallomics* **2011**, *3*, 1049–1055; c) O. Dömötör, C. G. Hartinger, A. K. Bytzeck, T. Kiss, B. K. Keppler, E. A. Enyedy, *J. Biol. Inorg. Chem.* **2013**, *18*, 9–17.
- [19] a) G. Sudlow, D. J. Birkett, D. N. Wade, *Mol. Pharmacol.* **1976**, *12*, 1052–1061; b) G. Sudlow, D. J. Birkett, D. N. Wade, *Mol. Pharmacol.* **1975**, *11*, 824–832.
- [20] L. Trynda-Lemiesz, B. K. Keppler, H. Kozłowski, *J. Inorg. Biochem.* **1999**, *73*, 123–128.
- [21] A. A. Batista, S. A. Onofre, S. L. Queiroz, G. Oliva, M. R. M. Fontes, O. R. Nascimento, *J. Braz. Chem. Soc.* **1997**, *8*, 641–647.
- [22] a) P. Mura, M. Camalli, L. Messori, F. Piccioli, P. Zanello, M. Corsini, *Inorg. Chem.* **2004**, *43*, 3863–3870; b) M. A. Jakupec, E. Reisner, A. Eichinger, M. Pongratz, V. B. Arion, M. Galanski, C. G. Hartinger, B. K. Keppler, *J. Med. Chem.* **2005**, *48*, 2831–2837; c) E. Reisner, V. B. Arion, A. Eichinger, N. Kandler, G. Giester, A. J. L. Pombeiro, B. K. Keppler, *Inorg. Chem.* **2005**, *44*, 6704–6716; d) E. Reisner, V. B. Arion, M. Fatima, C. G. da Silva, R. Lichtenecker, A. Eichinger, B. K. Keppler, V. Y. Kukushkin, A. J. L. Pombeiro, *Inorg. Chem.* **2004**, *43*, 7083–7093.
- [23] B. K. Keppler, W. Rupp, U. M. Juhl, H. Endres, R. Niebl, W. Balzer, *Inorg. Chem.* **1987**, *26*, 4366–4370.
- [24] O. M. Ni Dhubghaill, W. R. Hagen, B. K. Keppler, K. G. Lipponer, P. J. Sadler, *J. Chem. Soc. Dalton Trans.* **1994**, 3305–3310.
- [25] a) M. I. Webb, R. A. Chard, Y. M. Al-Jobory, M. R. Jones, E. W. Y. Wong, C. J. Walsby, *Inorg. Chem.* **2012**, *51*, 954–966; b) M. I. Webb, C. J. Walsby, *Dalton Trans.* **2011**, *40*, 1322–1331.
- [26] J. A. Weil, J. R. Bolton, *Electron Paramagnetic Resonance: Elementary Theory and Practical Applications*, 2nd ed., Wiley-Interscience, New York, **2007**.
- [27] B. Cebrián-Losantos, E. Reisner, C. R. Kowol, A. Roller, S. Shova, V. B. Arion, B. K. Keppler, *Inorg. Chem.* **2008**, *47*, 6513–6523.
- [28] M. Bacac, A. C. G. Hotze, K. van der Schilden, J. G. Haasnoot, S. Pacor, E. Alessio, G. Sava, J. Reedijk, *J. Inorg. Biochem.* **2004**, *98*, 402–412.
- [29] M. I. Webb, Simon Fraser University (Burnaby), **2013**.
- [30] a) J. M. Santos, C. Cipriano, R. B. Faria, J. D. Figueroa-Villar, *Can. J. Chem.* **1997**, *75*, 890–898; b) J. M. Santos, A. L. B. Formiga, J. D. Figueroa-Villar, *J. Mol. Struct.* **2002**, *608*, 143–149; c) J. M. Santos, R. R. da Silva, A. L. B. Formiga, L. W. Tinoco, J. D. Figueroa-Villar, *Chem. Phys.* **2004**, *306*, 143–151.
- [31] T. J. Siek, R. J. Osiewicz, *J. Forensic Sci.* **1975**, *20*, 18–37.
- [32] P. T. Manoharan, P. K. Mehrotra, M. M. Taquikha, R. K. Andal, *Inorg. Chem.* **1973**, *12*, 2753–2757.
- [33] K. Krogh-Jespersen, H. J. Schugar, *Inorg. Chem.* **1984**, *23*, 4390–4393.
- [34] a) S. Wanwimolruk, D. J. Birkett, P. M. Brooks, *Mol. Pharmacol.* **1983**, *24*, 458–463; b) G. J. Quinlan, G. S. Martin, T. W. Evans, *Hepatology* **2005**, *41*, 1211–1219; c) G. Colmenarejo, *Med. Res. Rev.* **2003**, *23*, 275–301.
- [35] a) J. Szpunar, A. Makarov, T. Pieper, B. K. Keppler, R. Lobinski, *Anal. Chim. Acta* **1999**, *387*, 135–144; b) K. Poleć-Pawlak, J. K. Abramski, O. Semenova, C. G. Hartinger, A. R. Timerbaev, B. K. Keppler, M. Jarosz, *Electrophoresis* **2006**, *27*, 1128–1135.
- [36] a) J. Ghuman, P. A. Zunszain, I. Petitpas, A. A. Bhattacharya, M. Otagiri, S. Curry, *J. Mol. Biol.* **2005**, *353*, 38–52; b) I. Sjöholm, B. Ekman, A. Kober, I. Ljungstedtpahlman, B. Seiving, T. Sjödin, *Mol. Pharmacol.* **1979**, *16*, 767–777.
- [37] a) F. Kratz, B. Elsadek, *J. Controlled Release* **2012**, *161*, 429–445; b) B. Elsadek, F. Kratz, *J. Controlled Release* **2012**, *157*, 4–28.
- [38] a) F. Kratz, *J. Controlled Release* **2008**, *132*, 171–183; b) A. Wunder, U. Müller-Ladner, E. H. K. Stelzer, J. Funk, E. Neumann, G. Stehle, T. Pap, H. Sinn, S. Gay, C. Fiehn, *J. Immunol.* **2003**, *170*, 4793–4801; c) E. A. Murphy, B. K. Majeti, R. Mukthavaram, L. M. Acevedo, L. A. Barnes, D. A. Cheresch, *Mol. Cancer Ther.* **2011**, *10*, 972–982.
- [39] L. Kersten, H. Braunlich, B. K. Keppler, C. Gliessing, M. Wendelin, *J. Westphal, J. Appl. Toxicol.* **1998**, *18*, 93–101.
- [40] C. A. Smith, A. J. SutherlandSmith, B. K. Keppler, F. Kratz, E. N. Baker, *J. Biol. Inorg. Chem.* **1996**, *1*, 424–431.
- [41] J. R. Winkler, H. B. Gray, *Chem. Rev.* **1992**, *92*, 369–379.
- [42] Y. Song, M. R. Gunner, *J. Mol. Biol.* **2009**, *387*, 840–856.
- [43] a) M. Brindell, I. Stawoska, J. Supel, A. Skoczowski, G. Stochel, R. van Eldik, *J. Biol. Inorg. Chem.* **2008**, *13*, 909–918; b) L. Messori, P. Orioli, D. Vullo, E. Alessio, E. Iengo, *Eur. J. Biochem.* **2000**, *267*, 1206–1213.
- [44] P. Heffeter, M. Pongratz, E. Steiner, P. Chiba, M. A. Jakupec, L. Elbling, B. Marian, W. Korner, F. Sevelde, M. Micksche, B. K. Keppler, W. Berger, *J. Pharmacol. Exp. Ther.* **2004**, *312*, 281–289.
- [45] a) B. K. Keppler, W. Rupp, *J. Cancer Res. Clin. Oncol.* **1986**, *111*, 166–168; b) M. R. Berger, F. T. Garzon, B. K. Keppler, D. Schmaehl, *Anticancer Res.* **1989**, *9*, 761–765.
- [46] G. C. V. Tuan Giam Chuang, U. Kragh-Hansen, M. Otagiri, *Pharm. Res.* **2002**, *19*, 569–577.
- [47] a) A. Galeano, M. R. Berger, B. K. Keppler, *Arzneim.-Forsch.* **1992**, *42-1*, 821–824; b) C. Anderson, *Can. J. Chem.* **2001**, *79*, 1477–1482; c) P. Mura, F. Piccioli, C. Gabbiani, M. Camalli, L. Messori, *Inorg. Chem.* **2005**, *44*, 4897–4899; d) A. Nikolova, D. Ivanov, R. Buyukliev, S. Konstantinov, M. Karaivanova, *Arzneim.-Forsch.* **2001**, *51*, 758–762.
- [48] P. W. Betteridge, J. R. Carruthers, R. I. Cooper, K. Prout, D. J. Watkin, *J. Appl. Crystallogr.* **2003**, *36*, 1487.
- [49] L. J. Farrugia, *J. Appl. Crystallogr.* **1997**, *30*, 565.
- [50] WINEPR SimFonia, V. 1.26, Bruker Analytik GmbH, Copyright 1994–1997.

Received: July 9, 2013
Published online: November 7, 2013